This article has been accepted for publication in IEEE Transactions on Energy Conversion. This is the author's version which has not been fully edited and content may change prior to final publication. Citation information: DOI 10.1109/TEC.2023.3311460

Hybrid Physics-Based and Data-Driven Prognostic for PEM Fuel Cells Considering Voltage Recovery

Hangyu Wu, Wei Wang, Yang Li, *Member, IEEE*, Wenchao Zhu, Changjun Xie, *Member, IEEE,* Hoay Beng Gooi, *Fellow, IEEE*

***Abstract*—Predicting the degradation behaviors is challenging and essential for prognostics and health management for proton exchange membrane fuel cells (PEMFCs). However, existing methods based on data-driven or model-based methods can face the problem of significant performance inconsistencies in different prediction stages. We investigate the cause and attribute it to the ignorance of the voltage recovery phenomena of PEMFCs observed during the frequent start-stop processes during practical applications. A novel prognostic method is proposed to provide a more comprehensive analysis of PEMFC aging that integrates data-driven and model-based methods. Specifically, a physics-based aging model considering voltage recovery (PA-VR) is first reported as a model-based method to enhance the prediction effect at voltage mutation points. Then, the moving window method with iterative function is used to combine the data-driven method with the PA-VR model, which realizes the online update of model parameters. Finally, the weightings on individual approaches are dynamically determined at different stages throughout the PEMFC lifecycle. The proposed hybrid method achieves an effective improvement in prediction performance by combining the overall degradation trend predicted by the PA-VR model and the local dynamic characteristics predicted by the data-driven method.**

***Index Terms*—Fuel cell, aging prediction, hybrid method, voltage recovery.**

I. Introduction

Proton exchange membrane fuel cells (PEMFCs) are highly efficient and environmentally friendly power sources that make them a perfect fit for various modern sustainable applications, such as electrified transportation and power-to-gas systems [1],[2]. The PEMFC is well-suited for heavy-duty electric vehicles because of their lightweight construction and high energy efficiency [3],[4]. However, limited lifetime significantly hinders their large-scale integration into transportation and power systems [5],[6],[7]. Despite experimental tests suggesting longer lifetimes, the fast degradation of PEMFCs during practical use is attributed to the complex and constantly changing operating conditions and the absence of well-design prognostics and health management (PHM) systems [8]. Developing robust PHM systems is essential for extending the remaining useful life (RUL) of PEMFCs [9]. Thus, more advanced algorithms can be designed for energy management and control purposes [10],[11].

The prognostic algorithms of PEMFCs can be divided into three categories: Data-driven, model-based, and hybrid methods [12]. *Model-based methods* mainly adopt the mechanistic and empirical aging models. For example, Zhang *et al.* [13] proposed a model to describe the relationship between the external environment and the internal state of fuel cells. The unscented Kalman filter (UKF) was used for damage tracking and aging prediction of the PEMFC. Since fuel cells have highly complex and uncertain aging mechanisms, it is very challenging to establish a reliable mechanistic or physics-based aging model for real prognostic applications. Therefore, the empirical aging model-based prognostic method is more widely preferred for the degradation prediction of fuel cells in practice. For instance, Jouin *et al.* [14] proposed a prognostics framework that combines particle filtering with empirical models. Then, the RUL of the PEMFC is estimated through the probability distribution. Unfortunately, these empirical models cannot directly reflect the internal aging-related parameters. Therefore, the semi-empirical model considering the internal parameters of PEMFC becomes the research focus. A semi-empirical model was proposed in [15] by considering the degradation of components and validated on four datasets based on the particle filter. Another semi-empirical model was investigated in [14]. The health index and the uncertainty in the degradation process are estimated by the extended Kalman filter (EKF), and finally, the RUL is calculated. The voltage recovery phenomena are often ignored in model-based methods [14],[15],[16],[17].

In recent years, *data-driven methods* have received increasing research attention due to the advancements in artificial intelligence and data science. These methods use deep

This work was supported by the National Key Research and Development Program of China (2020YFB1506802), the Key Research and Development Project of Guangdong Province (2020B0909040004) and the Office of Naval Research Global (ONRG), USA under CODE 33D, Naval Energy Resiliency and Sustainability in Broad Agency Announcement N00014-18-S-B001, and ONRG award number: N62909-19-1-2037.

H. Wu and C. Xie are with the School of Automation, Wuhan University of Technology, Wuhan 430070, China and also with Hubei Key Laboratory of Advanced Technology for Automotive Components, Wuhan University of Technology, Wuhan 430070, China (email: jackxie@whut.edu.cn).

W. Wang is with the School of Hubei Key Laboratory of Advanced Technology for Automotive Components, Wuhan University of Technology, Wuhan 430070, China.

Y. Li is with the Department of Electrical Engineering, Gothenburg, 41296, Sweden (yangli@ieee.org).

W. Zhu is with State Key Laboratory of Advanced Technology for Materials Synthesis and Processing, Wuhan 430070, China and also with Hubei Provincial Key Laboratory of Fuel Cells, Wuhan 430070, China (email: zhuwenchao@whut.edu.cn).

H. B. Gooi is with the School of Electrical and Electronic Engineering, Nanyang Technological University, Singapore 639798, Singapore.

learning to build black-box models that can predict the RUL of PEMFCs without the need for an aging mechanism [18]. For example, based on a relevance vector machine (RVM), a remaining life prediction model of PEMFC was proposed by Wu *et al.* [19], who proved its advantages over the classical support vector machine (SVM) in a small training set. Furthermore, Zhou *et al.* [20] proposed a novel multi-stage prognostic approach to predict fuel cell performance and RUL accurately. Liu *et al.* [21] proposed a recurrent neural network (RNN) method that employed regular interval sampling and locally weighted scatterplot smoothing for data reconstruction and smoothing. The method subsequently utilized the long short-term memory (LSTM) approach for prediction, which improved the prediction accuracy by 28.46% compared to the BP neural network (BPNN). Based on reference [21], Long *et al.* [22] proposed a gated recurrent unit (GRU) with similar processing steps to LSTM but has a better performance. However, these methods require a large amount of experimental data to train the models and cannot make predictions based on fuel cell mechanisms. Furthermore, Wang *et al.* [23],[24] found that the performance of LSTM and GRU in multi-step prediction was unsatisfactory. The lack of real-time data during the prediction phase prevents model updates and causes the predicted results to converge to a horizontal line, rendering degradation trend prediction unachievable.

As a means of addressing the limitations of individual approaches, *hybrid methods* have emerged as a popular area of research. By combining the strengths of multiple techniques, hybrid methods offer a more comprehensive and effective solution [25]. Ma *et al.* [26] used LSTM to predict the voltage value as the observed value for EKF. Using the EKF, the voltage prediction value is determined by the PEMFC of internal aging parameters. Zhou *et al.* [27] proposed a hybrid forecasting architecture based on the moving window (MW) method and verified it under three datasets simultaneously. In [18], the degradation of fuel cells is divided into irreversible and reversible degradation processes, and the Kalman filter and neural network were used to predict degradation, respectively. This hybrid method could get detailed voltage recovery information and aging trends. Wang et al. [28] propose a hybrid prediction framework that combines a semi-empirical model and a data-driven method (DDM) with a sliding window. The semi-empirical model predicts the overall degradation trend, while the DDM predicts local change performance, achieving accurate short-term and long-term predictions in total. Tian et al. [29] proposed a hybrid prediction method that combines nonlinear autoregressive neural network (NARNN) with LSTM recurrent neural network. The decomposition of aging data based on empirical mode decomposition (EMD) enabled targeted selection of data-driven methods for prediction, leading to improved prediction accuracy.

In the methods mentioned above, the accuracy of the prediction is often inversely proportional to the length of the prediction period. Real-time updating of model parameters is crucial during prediction, particularly when dealing with limited data storage and computational capabilities. The predictive accuracy can be improved by constantly adjusting the model parameters based on incoming data, and the system can adapt to changing conditions under continuous processes. However, real-time updating strategies can encounter problems with frequent start-stop processes, creating vastly different operating conditions between stages affected by voltage recovery (VR). It was found that the voltage recovery can be characterized by a double exponential trend over time, which be combined with a model-based method to enhance the prediction accuracy [23].

In order to achieve the optimal level of prediction accuracy at each stage, a hybrid approach that leverages the best characteristics of individual methods is often the most effective. Building on the challenges and opportunities outlined above, this study presents an innovative online prediction framework for fuel cells. The framework combines a physical aging (PA) model, which takes into account the VR phenomenon and is based on empirical equations to capture overall decay trends, with a GRU model that enhances nonlinear predictive performance. Furthermore, in order to enhance the predictive accuracy of nonlinear information, this study incorporates an attention mechanism into the GRU model. This mechanism allows the model to focus on the most critical information in the input sequence, thus improving the overall accuracy of predictions. To ensure that predictions are made in real-time, a moving window method is used in combination with the attention-enhanced GRU model. This approach enables the model to process incoming data in small, overlapping windows, allowing for continuous online prediction. The weight assignment calculation of each model is also optimized to improve the accuracy and efficiency of the prediction process. The proposed methods improve the prediction accuracy by specifically addressing the following problems:

1) Combining the PA-VR model with an adaptive unscented Kalman filter (AUKF) mitigates the effect of frequent start-stop points on local prediction.

2) By incorporating the GRU with the attention mechanism, the general nonlinear trends not covered in the models can be considered.

3) With dynamic weight assignment, high robustness is introduced so that the advantages and disadvantages of the PA-VR and GRU models are optimally balanced.

The rest of the paper is organized as follows. In Section II, the hybrid prediction method and the models involved are introduced. In Section III, the raw data sources and experimental configurations are presented. In Section IV, the prediction results are presented and discussed. The concluding remarks are given in Section V.

II. Hybrid Prognostic Method

A. Hybrid Prognostic Framework

The proposed hybrid prediction framework is shown in Fig. 1. It consists of three steps: 1) Windowing the data; 2) Iterative training of model parameters for PA-VR model and GRU; 3) Computing weights for hybrid forecasting. Specifically, first, an online data acquisition platform is used to collect output voltage data. Second, the data preprocessing and window division are performed simultaneously, and real-time measurements are also used as the input of the PA-VR and the GRU for model retraining. Finally, the weights for different methods in each

This article has been accepted for publication in IEEE Transactions on Energy Conversion. This is the author's version which has not been fully edited and content may change prior to final publication. Citation information: DOI 10.1109/TEC.2023.3311460

window are calculated to obtain a final hybrid prediction result. With the moving window, the model parameters can be iteratively updated for real-time aging predictions.

Under the hybrid prediction framework, less training data are needed for online operation. The corresponding weighting factors can be dynamically adjusted by iteratively inputting real-time data to update the models of each method. The forecast duration at each step can be easily changed with different window horizons. Furthermore, the proposed method could predict the aging process more accurately during start-stop operation, providing more valuable information for decision-making.

B. *Model-Based Prediction Method*

a) PA model: The PA model predicts the primary aging trend of fuel cells. The stack voltage is modeled by considering the polarization parameters [30]:

$$V_{stack} = n_{cell} \times \left(E_{ocv} - Ri - aT\ln\left(\frac{i}{i_0}\right) + bT\ln\left(1 - \frac{i}{i_L}\right)\right) \tag{1}$$

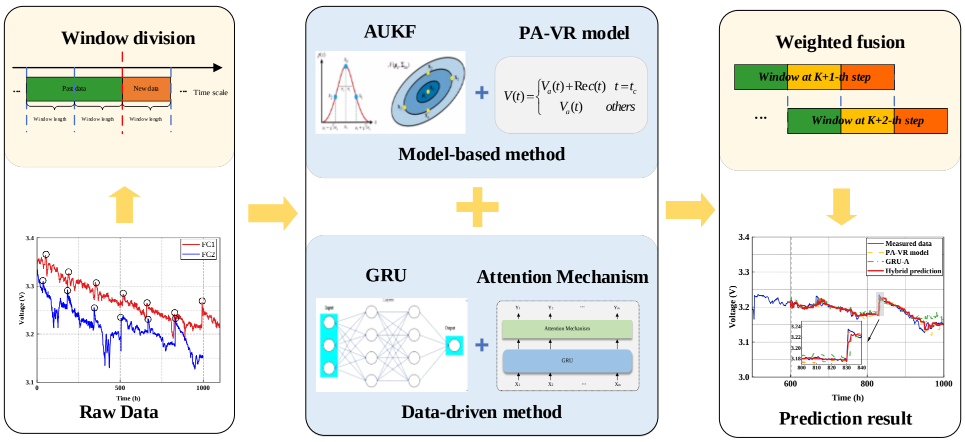

Fig. 1. Proposed Hybrid prediction framework for PEMFC aging prediction.

where V_{stack} is the output voltage, i is the current density, T is the operating temperature, and n_{cell} is the number of cells. a and b are the Tafel constant and the concentration constant, respectively. E_{ocv} is the open-circuit voltage, i_0 is the exchange current density, R is the area-specific resistance, and i_L is the limiting current density.

Over the fuel cell lifetime, E_{ocv} and i_0 can be treated as constants. R and i_L may change significantly under different currents due to the degradation of the membrane and bipolar resistance [31]. Therefore, R and i_L are selected as the aging parameters of the model. Moreover, Bressel *et al.* [32] found that a single parameter α can characterize the changing rate of R and i_L during the aging process. α can also reflect the downward trend in voltage, i.e.,

$$\begin{cases} R = R_0(1+\alpha(t)) \\ i_L = i_{L0}(1-\alpha(t)) \\ \alpha(t) = \beta(t)\times t \end{cases} \tag{2}$$

where β represents the aging rate of α, the least squares method can be used to determine α based on the polarization curve at the initial time [15]. Combining (1) and (2) yields the PA model

$$V_a(t) = N\cdot\left(E_{ocv} - R_0(1+\alpha(t))i(t) - aT\ln\left(\frac{i(t)}{i_0}\right) + bT\ln\left(1-\frac{i(t)}{i_{L0}(1-\alpha(t))}\right)\right) \tag{3}$$

b) PA-VR model: A recovery in the output voltage of fuel cells can always be observed after the start-stop operation, which leads to a degree of bias in predictions. Since the PA model (3) only describes irreversible aging behaviors, it can only be used to predict the overall downward trend in the terminal voltage during aging, whereas the information regarding voltage recovery due to reversible aging mechanisms is ignored [33]. Therefore, a VR model is needed for enhanced voltage prediction.

By extracting the features of the existing VR phenomenon, VR can be predicted at any start-stop point using the VR model. A double exponential empirical model is adopted [34]:

$$\mathrm{Rec}(t) = r_1\cdot\exp(r_2\cdot t) + r_3\cdot\exp(r_4\cdot t) \tag{4}$$

where r_1-r_4 are VR model parameters, which can be obtained by fitting the difference in predicted and measured voltage data between start-stop points.

The PA-VR model is obtained by combining (3) and (4):

$$V(t) = \begin{cases} V_a(t) + \mathrm{Rec}(t) & t = t_c \\ V_a(t) & \text{otherwise} \end{cases} \tag{5}$$

where t_c represents the time of the preset start-stop point.

With the VR model determined during the training phase, only the prediction part needs to be changed. Fig. 2 illustrates the workflow of the VR model. According to the model parameters obtained in the training process, the state information is transmitted through the empirical model. When the start-stop point t_c is reached during the prediction process, the VR model is added.

This article has been accepted for publication in IEEE Transactions on Energy Conversion. This is the author's version which has not been fully edited and content may change prior to final publication. Citation information: DOI 10.1109/TEC.2023.3311460

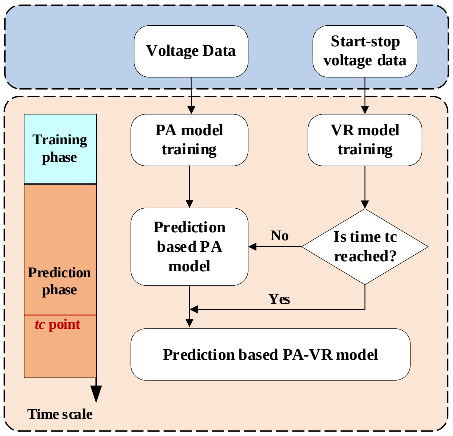

Fig. 2. Flow chart of combing PA and VR.

c) AUKF: To extract the aging parameters, the system can be converted to a nonlinear discrete-time system with sampling interval Δt (1 h in this work)

$$\begin{cases} x_k = Ax_{k-1} + n_{k-1} \\ y_k = h(x_k, u_k) + v_k \end{cases} \tag{6}$$

where $k = t/\Delta t$ is the discrete-time index, state $x = [\alpha, \beta]^T$ consists the aging parameters in (2), $y = V$ is the measured voltage, and the input $u = i$ is the current density. n and v are the process and measurement noises, respectively. A is the state transition matrix, and h is the measurement function determined by (3)-(5). This discrete-time state-space equation is given as

$$\begin{cases} \begin{bmatrix} \alpha_k \\ \beta_k \end{bmatrix} = \begin{bmatrix} 1 & \Delta t \\ 0 & 1 \end{bmatrix} \begin{bmatrix} \alpha_{k-1} \\ \beta_{k-1} \end{bmatrix} + n_{k-1} \\ y_k = \begin{cases} V_{a,k} + v_k & \text{otherwise} \\ V_{a,k} + r_1 \cdot \exp(r_2 \cdot t) + r_3 \cdot \exp(r_4 \cdot t) + v_k & t = t_c \end{cases} \end{cases} \tag{7}$$

To reduce the influence caused by non-stationary noise in the process and measurement, covariance matching is used to adjust the covariance matrices adaptively. The main steps of the AUKF algorithm are given as follows:

1) Initialization

$$\begin{cases} \hat{x}_{0|0} = E(x_0) \\ P_{0|0} = E\left[(x_0 - \hat{x}_0)(x_0 - \hat{x}_0)^T\right] \end{cases} \tag{8}$$

2) The unscented transformation is used to generate $(2n+1)$ sigma points:

$$\begin{cases} \hat{x}^{(i)}_{k-1|k-1}, i = 0 \\ \hat{x}^{(i)}_{k-1|k-1} + \left(\sqrt{(n+\lambda)\hat{P}_{x,k-1|k-1}}\right)^{(i)}, \quad i = 1 \ldots n \\ \hat{x}^{(i)}_{k-1|k-1} - \left(\sqrt{(n+\lambda)\hat{P}_{x,k-1|k-1}}\right)^{(i)}, \quad i = n+1 \ldots 2n \end{cases} \tag{9}$$

3) Update of predicted state $x^{(i)}_{k|k-1}$ and prior error covariance $\hat{P}_{x,k|k-1}$

$$x^{(i)}_{k|k-1} = Ax^{(i)}_{k-1|k-1} \tag{10}$$

$$\hat{x}_{k|k-1} = \sum_{i=0}^{2n} w^{(i)}_m x^{(i)}_{k|k-1} \tag{11}$$

$$\hat{P}_{x,k|k-1} = \sum_{i=0}^{2n} w^{(i)}_c \left(x^{(i)}_{k|k-1} - \hat{x}_{k|k-1}\right)\left(x^{(i)}_{k|k-1} - \hat{x}_{k|k-1}\right)^T + Q_{k-1} \tag{12}$$

4) Compute the Kalman gain, and update the system state and error covariance from measurements:

$$K = \hat{P}_{xy,k|k-1}\hat{P}^{-1}_{yy,k|k-1} \tag{13}$$

$$Q_k = KF_k K^T \tag{14}$$

$$\hat{x}_{k|k} = \hat{x}_{k|k-1} + K\left(y_k - \hat{y}_{k|k-1}\right) \tag{15}$$

$$\hat{P}_{x,k|k} = \hat{P}_{x,k|k-1} - K\hat{P}_{yy,k|k-1}K^T \tag{16}$$

C. *Data-Driven Prognostic Method*

GRU is to improve the effect of long sequence prediction [35]. As shown in Fig. 3(a), GRU has two gate functions: the update gate $z(t)$ and the reset gate $r(t)$. The GRU is described by

$$z(t) = \sigma(W_z \bullet [H(t-1), X(t)]) \tag{17}$$

$$r(t) = \sigma(W_r \bullet [H(t-1), X(t)]) \tag{18}$$

$$\hat{H}(t) = \tanh(W_H [r(t) \bullet H(t-1), X(t)]) \tag{19}$$

$$H(t) = (1 - z(t)) \bullet H(t-1) + z(t) \bullet \hat{H}(t) \tag{20}$$

$$Y(t) = \sigma[W_Y H(t) + b_Y] \tag{21}$$

where W_z, W_r, and W_H are the network weights of the update gate, reset gate, and candidate states, respectively. $z(t)$ is the update gate; $r(t)$ is the reset gate; and $H(t)$ is the hidden state. It can be seen from (17) that GRU can forget and select using the same gate $z(t)$ (LSTM needs to use multiple gates) and realizes the optimization of the structure. The output $Y(t)$ of the current neuron is obtained by (21).

The attention mechanism is introduced into the GRU to improve the prediction performance. Theoretically, the attention mechanism can be used before or after the GRU method. However, using it before the GRU method would cause part of the attention to be distracted by other features, resulting in a decline in the effectiveness of the method. So this paper uses the attention mechanism after the GRU method [36]. The input layer processes the input voltage data into multiple feature vectors for GRU training. Then the feature vectors are inputted into the hidden layer for the GRU model training to get the initial output vectors. In order to obtain a reasonable attention distribution, the initial output vectors are used as the input vectors of the attention mechanism, and the attention weight parameters are calculated. Finally, the final predicted value is obtained by the output layer. The structure of GRU with attention mechanism (GRU-A) is shown in Fig. 3(b).

The numbers of input, hidden, and output layers of the GRU are selected as 1, 2, and 1, respectively. The input layer has 60 neurons, each with 100 weights and 100 biases. The first hidden layer has 100 neurons, and each neuron has 80 weights and 80 biases. The second hidden layer has 80 neurons, each with 10 weights and 10 biases. Finally, the output layer has 10 neurons, each containing 1 weight parameter and 1 bias parameter. Introducing the attention mechanism to the GRU increases the attention calculation without affecting the parameter settings of other links in the GRU.

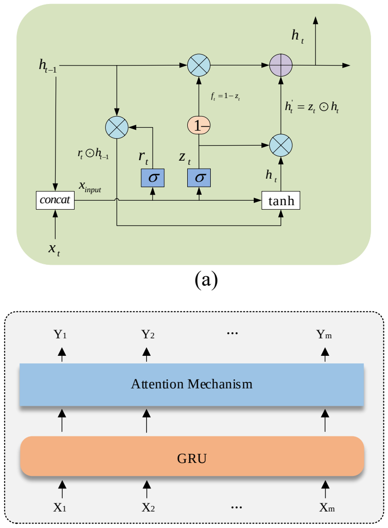

(a)

(b)

Fig. 3. (a) Basic GRU structure. (b) GRU with the attention mechanism.

D. Moving Window Method

With the MW method, the PA-VR model and the data-driven model can be iteratively trained the by the latest data. The MW method provides dynamic weights and thresholds of each model to increase the prediction accuracy. To achieve iterative training in degradation prediction, the input dataset is continuously updated through the MW, as shown in Fig. 4.

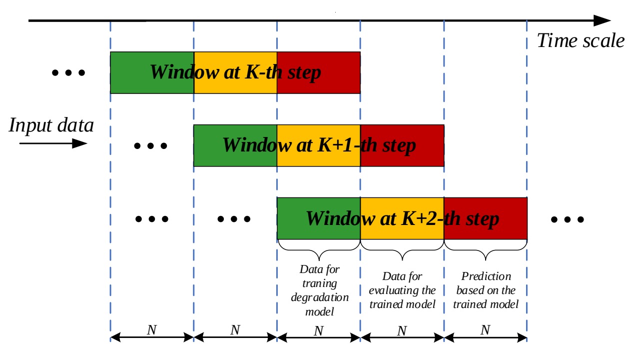

Fig. 4. Moving window method.

Each step is composed of three parts: the training phase (green area), the update phase (yellow area), and the prediction phase (red area). In the green area, the PA-VR model and GRU-A are trained by the measured data in each prediction process. In the yellow area, the weight factor of each method is calculated based on the newly measured and predicted data. The hybrid prediction result is obtained in the red area by combining each method with its corresponding weighting factor.

To illustrate the MW method, three consecutive MWs are defined in the *K*th step as *N*, *N*+1, and *N*+2. In the first step, the output voltage data is preprocessed, and the window is divided. To incorporate aging information of the current stage, the PA-VR model and the GRU-A model are both trained by the real-time data collected in the current window *N*. When the PA-VR model predicts the start-stop point t_c in the future windows *N*+1 and *N*+2, the VR model needs to be added, and the remaining voltage predictions must be performed simultaneously in these windows. Then, weight calculations are performed on the actual and predicted value of window *N*+1, respectively. Finally, the hybrid prediction result is obtained by combining the weight factor with the predicted value in window *N*+2. During the *K*=1 step, the real values of the two windows are used to calculate the weight for the training and updating parts of the model. However, each of the remaining steps only requires the input of one window length online. The flowchart of the hybrid prediction framework is shown in Fig. 5.

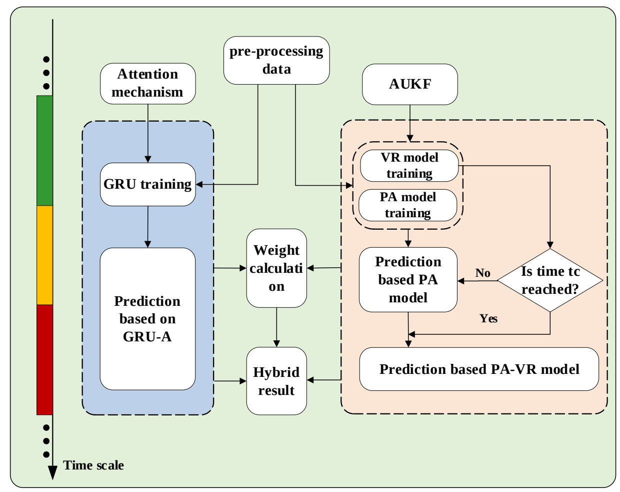

Fig. 5. Flow chart of proposed hybrid method

In the update phase, the real-time voltage data are compared with the predicted value of each method in the current period, which is used to calculate the weight of each method in the hybrid process at the current step. Considering that *M* models are used in the hybrid framework, leading to the following expression.

$$\omega_l = \frac{1}{\sum_{i=1}^{N}\sqrt{\left(y(i)-\hat{y}_{eva,l}(i)\right)^2}} \quad (l=1,2,\cdots,M) \tag{22}$$

where ω_l represents the weight factor of the *l*-th model in the hybrid model framework (for the present investigation, $l = 1$ for the PA-VR model, $l = 2$ for the GRU-A model, and $M = 2$) at the current step *K*. Furthermore, *y* is the measured voltage and $\hat{y}_{eva,l}$ represents the predicted voltage from the *l*-th model. After the weight factors are obtained, normalization and weighted summation are performed to obtain the fused prediction:

$$\omega_{norm,l} = \frac{\omega_l}{\sum_{l=1}^{M}\omega_l} \tag{23}$$

$$y_{fus} = \sum_{l=1}^{M}\left(\hat{y}_{eva,l}\cdot\omega_{norm,l}\right) \tag{24}$$

III. Data Description

The aging datasets used in this paper are collected for static load and dynamic load, respectively [37]. PEMFC is tested for 1100 hours under a static load and 1000 hours under a dynamic load. The first fuel cell, FC1, undergoes an aging test under a

This article has been accepted for publication in IEEE Transactions on Energy Conversion. This is the author's version which has not been fully edited and content may change prior to final publication. Citation information: DOI 10.1109/TEC.2023.3311460

constant current density of 0.7 A/cm², while the second fuel cell, FC2, is tested under the same current density with a frequency of 5 kHz and a current ripple of 10%. Considering that the raw voltage data may contain some noise and sharp peaks, the calculation time would increase due to the large number of points collected. Each data point is 1 hour apart.

During the operation of PEMFCs, it is necessary to interrupt the operation for electrochemical impedance spectroscopy (EIS) and polarization curve tests, resulting in multiple start-stop points. As shown in Fig. 6, at the above-mentioned start-stop points, the output voltage of the fuel cell will recover significantly [38].

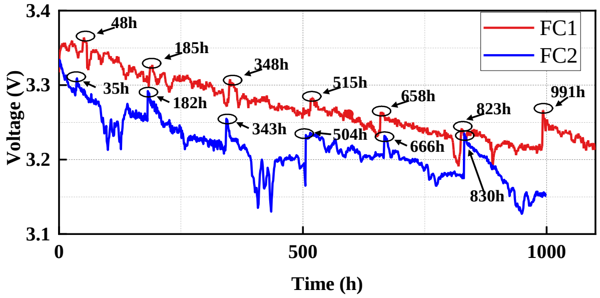

Fig. 6. Voltage degradation curve.

IV. Results and Discussion

Predictive models can be evaluated based on two commonly used criteria. They are the mean absolute percentage error (MAPE) and root mean square error (RMSE):

$$\mathrm{MAPE}=\frac{1}{N}\sum_{t=1}^{N}\frac{|y(t)-\hat{y}(t)|}{|y(t)|} \tag{25}$$

$$\mathrm{RMSE}=\sqrt{\frac{1}{N}\sum_{t=1}^{N}(y(t)-\hat{y}(t))^2} \tag{26}$$

where $y(t)$ is the measured voltage; $\hat{y}(t)$ is the voltage predicted; $\bar{y}(t)$ is the average value; and N is the number of voltage data.

A. *Performance of the PA-VR Model*

To present the advantages of the PA-VR model, different models with AUKF are used for prediction under static and dynamic load conditions, respectively. Meanwhile, the MW method is added to the PA-VR model, and the model parameters can be updated iteratively, further improving the prediction accuracy. Experiments are conducted under static and dynamic loads to analyze the impact of voltage recovery on the prediction effect.

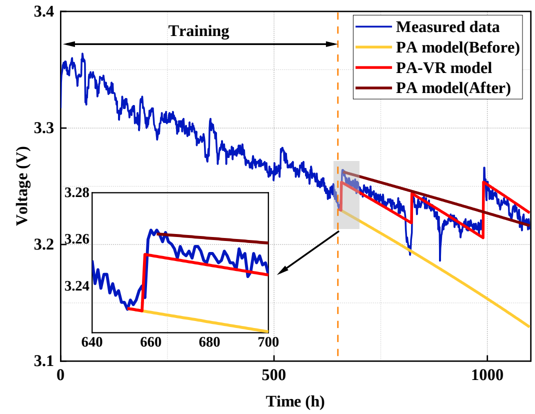

(a)

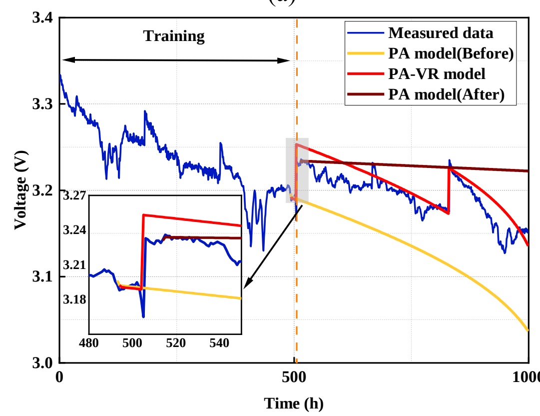

(b)

Fig. 7. Model-based prediction results of (a) FC1 and FC2.

As shown in Fig. 7(a), the experiment under static load on FC1 is conducted over 1100 hours. Based on the PA-VR model, the prediction starts at 652 h, and three future start-stop points are included. The effect of the prediction is shown as the red curve. Both the yellow and brown curves are PA model predictions. The difference is that the prediction starts before and after the fifth start-stop point (658 h). The RMSEs of the PA model (before) and PA-VR model are 0.0562 and 0.0087, respectively, which reduced by 84.5%. The prediction points of the yellow and brown are only 10 hours apart (prediction point before the start-stop point: 652 h, prediction point after the start-stop point: 662 h). However, the prediction results have a significant deviation. The yellow curve is below the actual data (blue line), making fuel cell aging tracking impossible. Even though the brown curve tracks the aging trend better than the yellow curve, it cannot predict fluctuations in the voltage caused by recovery. The partially enlarged picture in Fig. 8 shows that the red curve predicts the recovery voltage of the start-stop point and follows the future aging trend. Using the data of the start-stop point, the parameter information of the recovery phenomenon can be extracted by the PA-VR model.

In Fig. 7(b), the red curve shows the prediction effect based on the PA-VR model beginning at 495 h. The starting points of the yellow and brown prediction curves are before and after the fifth start-stop point (515 h). The RMSEs of the PA model (before) and PA-VR model are 0.0681 and 0.0185, respectively, which reduced by 72.8%. The yellow and brown prediction curves have quite different trends depending on the prediction

This article has been accepted for publication in IEEE Transactions on Energy Conversion. This is the author's version which has not been fully edited and content may change prior to final publication. Citation information: DOI 10.1109/TEC.2023.3311460

starting point. The recovery voltage cannot be presented in the PA model, which hinders the estimation of the aging index α when the voltage has just been recovered, resulting in a poor prediction effect of the brown curve. The prediction for the brown curve is almost horizontal, which is unreasonable for fuel cell aging. The yellow curve has been below real data, which cannot accurately predict future aging trends. The detail of Fig. 7(b) shows that the red curve effectively predicts the recovery voltage and follows the aging trend, which means the PA-VR model is capable of accurately predicting the voltage recovery process of the start-stop point.

To further illustrate the influence of the selected prediction points on the prediction results of the PA model, Fig. 8 shows the changes in the aging parameter α and its rate of change β with time for FC1 and FC2. It can be observed from the figure that the values of α are not the same at different time points, and the difference in values before and after the start-stop point is greater. However, in the prediction phase, the future aging trend is evaluated based on the last aging parameter obtained in the training phase. Therefore, the choice of the prediction starting point significantly influences the PA model's prediction effect, which cannot reflect voltage recovery information. Meanwhile, the prediction error of the PA-VR model will accumulate over time. Therefore, using more measured data over time can help adjust the aging parameters of the model, and selecting a moderate prediction step size helps achieve accurate online predictions. Hence, the MW is used to update aging parameters and adjust prediction step sizes iteratively.

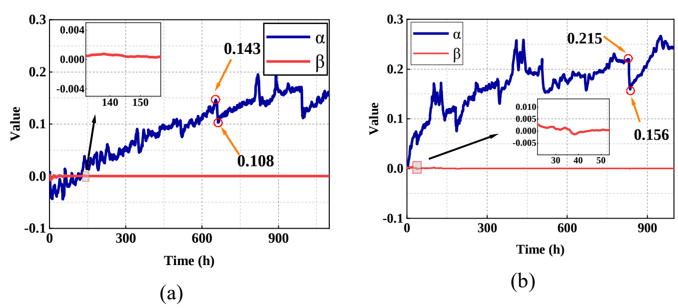

Fig. 8. Value of aging parameters for (a) FC1 and (b) FC2.

B. *Effect of the Moving Window*

To guarantee continuous updating of model parameters, the PA-VR model is enhanced by adding an MW with $N = 10$. Fig. 9(a) shows the prediction results of FC1. The red curve represents the prediction of the PA-VR model at 652 h (consistent with Section IV-A). The green curve represents the prediction results with MW, and the starting point for the prediction is 50 h. In the PA-VR model, more data are used (0-652 h) to train the model. With the MW method, the degradation model is dynamically updated with the updated measurement data during degradation prediction. Thus, the prediction is iterated from 50 h onwards. To analyze the advantages of the MW method, the prediction results with MW are also analyzed from 652 h to compare with those of the PA-VR model. As shown in the partially enlarged picture, the forecast trend (green curve) is no longer a simple continuous curve after adding the MW method but rather a gradual rise or fall in the prediction.

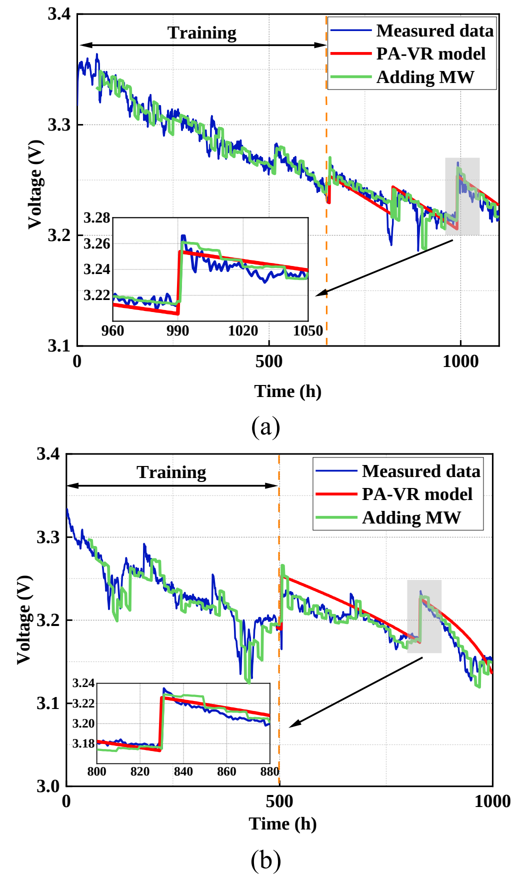

Fig. 9. Prediction results with MW of (a) FC1 and (b) FC2.

Fig. 9(b) shows the prediction results of FC2. The red curve represents the prediction results of the PA-VR model for the starting point at 505 h. The green curve represents the prediction results with MW, and the prediction starts at 50 h. To analyze the advantages of MW, its prediction results are compared with those of the PA-VR model. Due to the large voltage fluctuations under dynamic loads, the PA-VR model cannot predict voltage fluctuations during the aging process, even though the voltage recovery phenomenon of the start-stop point can be handled. In Fig. 9(b), the green curve in the enlarged part shows that the MW improves the voltage trend prediction.

Although the number of predictions increases, the prediction effect has been dramatically enhanced. The PA-VR model with the MW method can only track the overall aging trend (irreversible aging) but not the detailed information (reversible aging). The data-driven methods can predict detailed degradation information, including voltage fluctuations and stochastic information under operating conditions. For robustness and accuracy, it is essential to combine data-driven methods.

C. *Analysis of the hybrid prognostic method*

Considering both reversible and irreversible aging, the hybrid prognostic method with the MW is expected to obtain better results. To further demonstrate that the hybrid method can predict with fewer data, this section uses data from two time periods of the fuel cell: FC1 (500h-1100h) and FC2 (500h-1000h). The length of the training set is uniformly set to 100h.

The horizon of MW in each method is N=10. AUKF combines Bayesian theory for state estimation. Therefore, the aging indicator obtained is the optimal estimate value. However, the output results of the neural network model fluctuate within a certain range and are not a single deterministic value. In this section, the prediction of GRU-A is repeated fifty times, and the median of the prediction is calculated and plotted as a green line.

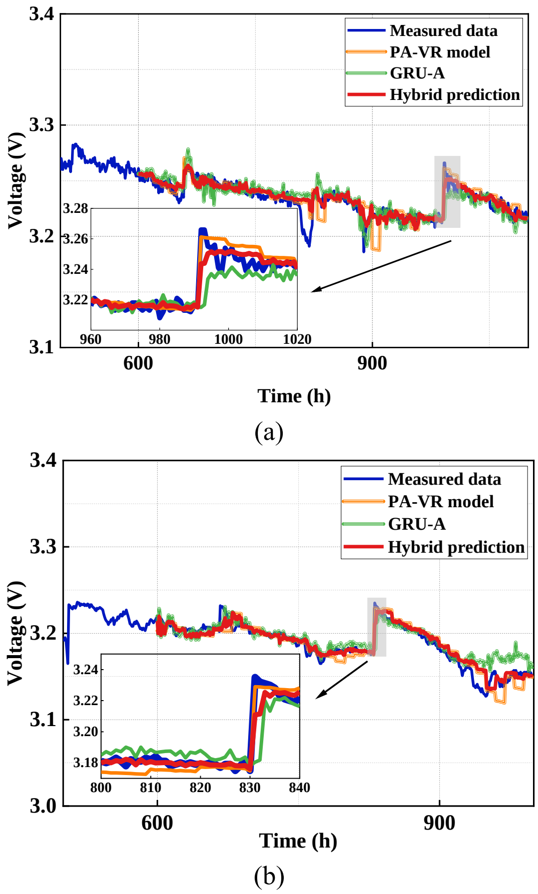

Fig. 10. Comparison of each prediction method results of (a) FC1 and (b) FC2.

Fig. 10(a) shows the hybrid prediction results of FC1. The hybrid prediction (red curve) is consistently positioned between the PA-VR model (yellow curve) and the GRU-A (green curve). When the training data for the model is limited, the GRU-A can still produce good results in multi-step predictions. In addition, the estimation results of the GRU-A are calculated based on multiple prediction results, which minimizes the uncertainty of the prediction results and leads to more accurate estimation results. The GRU-A effectively predicts voltage fluctuations and captures detailed degradation information over long periods without start-stop points. However, it is difficult for the data-driven method to predict the recovery voltage at the start-stop point, which the PA-VR model could effectively address. Meanwhile, the proposed hybrid method can increase the weight of the relatively accurate method to ensure high-accuracy results. By weighting the results, the inaccurate predictions of a single method are always balanced.

As shown in Fig. 10(b), the hybrid method would be even more effective under dynamic conditions. In the partially enlarged diagram, the proposed hybrid method has a superior prediction effect under dynamic loads, while the GRU-A shows an upward fluctuation trend during 960 h-1000 h. The data-driven approach enables the hybrid method to reliably predict voltage fluctuations without start-stop points. Generally, the hybrid method with MW can achieve accurate prediction near the start-stop point (830 h), and it also performs well in the period 960 h-1000 h.

To quantify the superiority of the hybrid method, Table I shows RMSE and MAPE (T_p=600 h). Compared to GRU-A, the hybrid method reduces the RMSE and MAPE of FC1 by 26.7% and 20.3%, respectively. For FC2, RMSE and MAPE of the hybrid method are reduced by 35.4% and 35.7%, respectively. The prediction accuracy has dramatically improved by combining the MW with the hybrid method. Considering both reversible and irreversible aging simultaneously, the hybrid method achieves significant accuracy improvements under dynamic load conditions.

The models have been executed in MATLAB 2021a on a laptop computer with a processor of 3.10 GHz and 16 GB RAM. From the perspective of computational efficiency, the PA-VR model requires less time compared to GRU-A. The PA-VR model is based on its own optimal estimation using AUKF, which has the efficiency of an unscented transform and adaptive parameter adjustment. On the other hand, GRU-A, essentially an RNN, is a deep learning model with a large number of parameters, and the selection of hyperparameters can also increase time costs. It is noteworthy that the computational efficiency of the hybrid method is basically the same as that of GRU-A, because the hybrid result is a weighted combination of the output from each individual method. As the aim of our work is to predict several tens of hours ahead, the time cost of the hybrid framework is acceptable and will not affect the maintenance operations of the personnel after the prediction.

TABLE I.
COMPARISON WITH A SINGLE METHOD

Dataset	Strategies	RMSE	MAPE	Time（s/MW）
FC1	PA-VR model	0.0095	0.0019	0.059
	GRU-A	0.0101	0.0021	14.806
	Hybrid prediction	0.0074	0.0015	15.955
FC2	PA-VR model	0.0101	0.0024	0.055
	GRU-A	0.0127	0.0028	14.032
	Hybrid prediction	0.0082	0.0018	15.124

D. *Analysis of different window lengths*

Selecting an appropriate window length can ensure accurate degradation prediction while providing sufficient diagnostic time for upcoming faults. With a longer window horizon N, more measured data would be used to train the model, resulting in a more accurate model. However, increasing the prediction length would reduce the accuracy of the results. Hence, different N (10, 20, 50) and forecast starting points (500 h, 600 h, 700 h, 800 h) are used in this section for analysis.

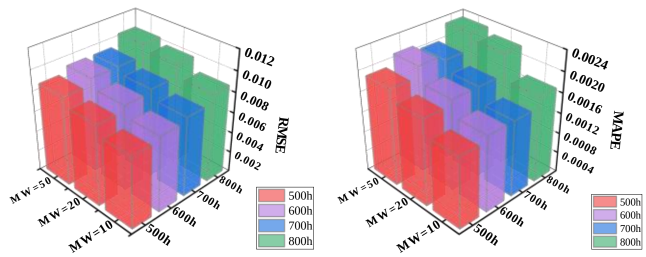

Fig.11. Prediction error of FC1 (a) RMSE (b) MAPE.

Fig. 11(a) shows the comparison results under different N for FC1. For RMSE and MAPE, the prediction error with N = 10 is the smallest at different forecast starting points. It represents a higher forecast accuracy in each period. Compared with a case with N = 50, the RMSE is lower by 19.5-20.4% and the MAPE decreased by 26.3-28.6%. For the N = 50, Fig. 11(b) shows that the numerical fluctuations of the adjacent prediction starting points are more pronounced, which means the longer the horizon, the less stable the forecast.

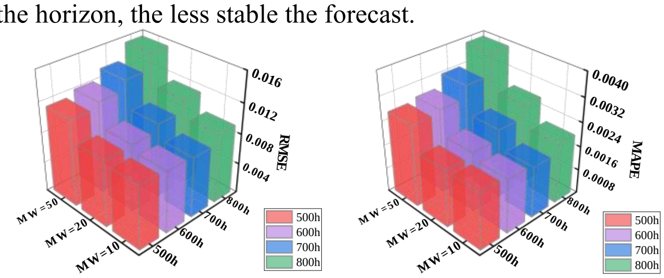

Fig.12. Prediction error of FC2 (a) RMSE (b) MAPE.

Fig. 12 shows the comparison results under different N for FC2. For RMSE and MAPE, the forecasting error for N = 10 is the smallest at different forecast starting points. The larger prediction error of FC2 is caused by the more fluctuating voltage of the dynamic load. Compared to N = 50, the RMSE of N = 10 has decreased by 26.3%~40.6%, and the MAPE decreased by 29.6%~48.7%. In addition, FC2 exhibits an apparent recovery phenomenon between 800 h to 1000 h. However, N = 10 is a more accurate predictor than other horizons in this period because of the reasonable window length.

When the fuel cell voltage fluctuates significantly, appropriate predicted step sizes can guarantee better prediction accuracy because it ensures the correlation between the two adjacent steps. Thus, better predictions can be achieved by adopting different window lengths for different types of fuel cell aging processes. The aging condition of the current fuel cell can be analyzed based on real-time data input. Generally, a significant fluctuation in the data often indicates a fault or instability in the system, and N needs to be reduced regularly to detect the fault [26]. Instead, the window length can be appropriately increased to predict the long-term trend of the equipment under historical operating conditions, and the control strategy can be adjusted following the expected trend. For the fuel cell data referenced in this paper, N = 10 can achieve a more accurate prediction while ensuring an appropriate prediction step size.

E. Comparison with other methods

Based on the moving window prediction, it is essentially an advanced multi-step prediction. To further validate the superiority of the hybrid method, this section compares and analyzes it with methods that conduct multi-step predictions in other literature. Meanwhile, the prediction results in Section 4.2 will be used for comparison. The RMSEs of different approaches are concluded in Table II.

TABLE II.
COMPARISON WITH DIFFERENT STRATEGIES

Strategies	FC1		FC2	
	n=10	n=15	n=10	n=15
LSTM[39]	0.0127	0.0172	0.0103	0.0136
BI-LSTM[39]	0.0067	0.0089	0.0095	0.0126
Dil-CNN-A[39]	0.0069	0.0086	0.0090	0.0118
Proposed hybrid prediction	MW=10	MW=20	MW=10	MW=20
	0.0073	0.0083	0.0081	0.0096
TCN-LSTM[40]	0.0099	0.0117		
BPNN-ANFIS[41]	0.0079		0.0123	
SE- NARNN-LSTM[29]			0.0091	

As shown in Table II, the hybrid method proposed in this paper is extensively compared with methods in existing work. Some methods are selected for comparative analysis.

Benaggoune *et al.* [39] proposed a data-driven method using a multi-step prediction mode and a dilated convolutional neural network (Dil-CNN) with an attention mechanism for predicting the performance of fuel cells for the first time. For FC1 prediction, it can be seen that Dil-CNN-A has slightly higher prediction accuracy than the hybrid method when the step size is 10. At a step size of 15, the RMSE of Dil-CNN-A is 0.0086, while the RMSE of the hybrid method at MW = 20 is 0.0083. Even with longer step sizes for each prediction, the hybrid method still achieves high prediction accuracy. For FC2 prediction, at a step size of 10, the hybrid method has a 10% higher prediction accuracy than Dil-CNN-A. Compared with the prediction result of Dil-CNN-A at a step size of 15, the hybrid method has an 18.6% improvement at a longer step size (MW = 20).

Zhang et al. [40] proposed a dual neural network cooperative prediction method. Based on the temporal convolutional network (TCN) for feature extraction, and LSTM is used to predict health indicators. From Table 2, it can be found that the prediction accuracy of the hybrid prediction framework proposed in this paper has an advantage under windows of different lengths. Accuracy increases by 26.2% and 29.1% with MW=10 and MW=20, respectively.

He et al. [41] investigated the impact of the historical behavior and operating modes of PEMFC on their future performance using back propagation neural network (BPNN) and adaptive neuro-fuzzy inference system (ANFIS). By calculating the weight of each model based on the corresponding prediction accuracy, the effectiveness of each factor was highlighted. With a window length of 10 hours, the proposed hybrid method improved the accuracy of FC1 and FC2 by 7.6% and 34.1%, respectively.

Tian et al. [29] proposed a hybrid prediction method that combines NARNN with LSTM recurrent neural network. The aging data was decomposed based on EMD, and the above data-driven methods were selectively used for prediction, ensuring the applicability of both data and algorithms. The proposed hybrid method in this paper improved the RMSE by 11.0% with a window of 10 hours for the FC2 dataset.

Compared to data-driven methods, the combination of model-based methods can improve prediction accuracy thanks to its ability to predict irreversible aging trends. The weight update of the moving window method can reduce the adverse impact of a single method when it makes poor predictions at a certain stage. In addition, the hybrid method uses only a small amount of real data (100h) for training in the first process, thus enabling online prediction.

V. Conclusion

Accurate degradation prediction is a prerequisite for estimating the RUL of fuel cells. The aim of this study is to develop a voltage hybrid prediction framework that combines model-based and data-driven methods to achieve more accurate predictions with less training data. The superiority of the proposed hybrid prediction method is demonstrated on an open-source dataset. In the model-based method, a PA-VR model that considers voltage recovery during the prediction phase is proposed. This effectively avoids the randomness caused by predicting before and after start-stop points, significantly improving prediction accuracy compared to classical physical polarization models. Furthermore, using a moving window method, the framework dynamically combines the GRU-A and PA-VR models. By iteratively updating the model parameters and adjusting the weights of the two models online, the prediction performance of the hybrid framework is significantly improved. The framework also exhibits high prediction accuracy at different window lengths. Additionally, the hybrid method outperforms the individual methods (PA-VR model and GRU-A), especially under dynamic operating conditions, reducing RMSE by 23.2% and 35.4% and MAPE by 25.0% and 35.7%, respectively.

However, there are still several issues that need to be analyzed and addressed in the future.

1) When predicting based on the PA-VR model using a shorter window length, the accuracy results are even better GRU-A. However, the model-based prediction is calculated based on the aging indicator and its change rate at the last moment. Therefore, when the window length is too long, the linearly expressed aging indicator cannot adequately reflect the voltage fluctuation at this stage, resulting in a poorer prediction effect for the PA-VR model. Proposing a new aging expression will become a research focus in future work.

2) Implementing online prediction requires algorithms with lower time cost during operation. The running speed of the data-driven method in the hybrid framework will affect the timeliness of online prediction. Further improving this issue can better achieve online prediction.

3) Currently, this article mainly predicts short-term and mid-term decay. As shown in Figures 10-11, the prediction performance of the hybrid method proposed in this article is also considerable under longer window lengths. In future work, this hybrid framework can be further studied for the remaining lifespan of fuel cells.

References

[1] K. Chen, S. Laghrouche, and A. Djerdir, 'Remaining Useful Life Prediction for Fuel Cell Based on Support Vector Regression and Grey Wolf Optimizer Algorithm', IEEE Transactions on Energy Conversion, vol. 37, no. 2, pp. 778–787, Jun. 2022.

[2] A. M. Dhirde, N. V. Dale, H. Salehfar, M. D. Mann, and T.-H. Han, 'Equivalent Electric Circuit Modeling and Performance Analysis of a PEM Fuel Cell Stack Using Impedance Spectroscopy', IEEE Transactions on Energy Conversion, vol. 25, no. 3, pp. 778–786, Sep. 2010.

[3] Q. Li et al., "An Energy Management Strategy Considering the Economy and Lifetime of Multi-Stack Fuel Cell Hybrid System," IEEE Trans. Transp. Electrific., pp. 1–1, 2022, doi: 10.1109/TTE.2022.3218505.

[4] Q. Li, P. Liu, X. Meng, G. Zhang, Y. Ai, and W. Chen, "Model Prediction Control-Based Energy Management Combining Self-Trending Prediction and Subset-Searching Algorithm for Hydrogen Electric Multiple Unit Train," IEEE Trans. Transp. Electrific., vol. 8, no. 2, pp. 2249–2260, Jun. 2022, doi: 10.1109/TTE.2022.3149479.

[5] T. Niu et al., "Study of degradation of fuel cell stack based on the collected high-dimensional data and clustering algorithms calculations," Energy and AI, vol. 10, p. 100184, Nov. 2022, doi: 10.1016/j.egyai.2022.100184.

[6] Z. Gong et al., "Adaptive optimization strategy of air supply for automotive polymer electrolyte membrane fuel cell in life cycle," Applied Energy, vol. 325, p. 119839, Nov. 2022, doi: 10.1016/j.apenergy.2022.119839.

[7] Z. Gong et al., "A 1 + 1-D Multiphase Proton Exchange Membrane Fuel Cell Model for Real-Time Simulation," IEEE Trans. Transp. Electrific., vol. 8, no. 2, pp. 2928–2944, Jun. 2022, doi: 10.1109/TTE.2021.3115794.

[8] Q. Li, L. Yin, H. Yang, T. Wang, Y. Qiu, and W. Chen, "Multiobjective Optimization and Data-Driven Constraint Adaptive Predictive Control for Efficient and Stable Operation of PEMFC System," IEEE Trans. Ind. Electron., vol. 68, no. 12, pp. 12418–12429, Dec. 2021, doi: 10.1109/TIE.2020.3040662.

[9] Y. Zou, Y. Xu, X. Feng, R. T. Naayagi, and B. Soong, "Transactive Energy Systems in Active Distribution Networks: A Comprehensive Review," CSEE Journal of Power and Energy Systems, vol. 8, no. 5, pp. 1302–1317, Sep. 2022, doi: 10.17775/CSEEJPES.2021.03290.

[10] D. Zhu et al., "Stochastic gradient-based fast distributed multi-energy management for an industrial park with temporally-coupled constraints," Applied Energy, vol. 317, p. 119107, Jul. 2022, doi: 10.1016/j.apenergy.2022.119107.

[11] D. Zhu, B. Yang, Y. Liu, Z. Wang, K. Ma, and X. Guan, "Energy management based on multi-agent deep reinforcement learning for a multi-energy industrial park," Applied Energy, vol. 311, p. 118636, Apr. 2022, doi: 10.1016/j.apenergy.2022.118636.

[12] W. Zhu et al., "Uncertainty quantification of proton-exchange-membrane fuel cells degradation prediction based on Bayesian-Gated Recurrent Unit," eTransportation, vol. 16, p. 100230, Apr. 2023, doi: 10.1016/j.etran.2023.100230.

[13] X. Zhang and P. Pisu, "Prognostic-oriented Fuel Cell Catalyst Aging Modeling and Its Application to Health-Monitoring and Prognostics of a PEM Fuel Cell," Int. J. Progno. Health Manag., vol. 5, no. 1, Art. no. 1, 2014.

[14] M. Jouin, R. Gouriveau, D. Hissel, M.-C. Péra, and N. Zerhouni, "Prognostics of PEM fuel cell in a particle filtering framework," Int. J. Hydrogen Energy, vol. 39, no. 1, pp. 481–494, Jan. 2014.

[15] M. Jouin, R. Gouriveau, D. Hissel, M.-C. Péra, and N. Zerhouni, "Degradations analysis and aging modeling for health assessment and prognostics of PEMFC," Rel. Eng. Syst. Safety, vol. 148, pp. 78–95, Apr. 2016, doi: 10.1016/j.ress.2015.12.003.

[16] M. Bressel, M. Hilairet, D. Hissel, and B. Ould Bouamama, "Remaining Useful Life Prediction and Uncertainty Quantification of Proton Exchange Membrane Fuel Cell Under Variable Load," IEEE Trans. Ind. Electron., vol. 63, no. 4, pp. 2569–2577, Apr. 2016.

[17] B. Xiao, J. Zhao, L. Fan, Y. Liu, S. H. Chan, and Z. Tu, "Effects of moisture dehumidification on the performance and degradation of a proton exchange membrane fuel cell," Energy, vol. 245, p. 123298, Apr. 2022, doi: 10.1016/j.energy.2022.123298.

[18] R. Ma, T. Yang, E. Breaz, Z. Li, P. Briois, and F. Gao, "Data-driven proton exchange membrane fuel cell degradation predication through deep learning method," Applied Energy, vol. 231, pp. 102–115, Dec. 2018.

[19] Y. Wu, F. Gao, D. Paire, A. Miraoui, and E. Breaz, "Nonlinear Performance Degradation Prediction of Proton Exchange Membrane Fuel Cells Using Relevance Vector Machine," IEEE Transactions on Energy Conversion, vol. 31, no. 4, pp. 1570–1582, Dec. 2016.

[20] D. Zhou, A. Al-Durra, K. Zhang, A. Ravey, and F. Gao, "Online remaining useful lifetime prediction of proton exchange membrane fuel cells using a novel robust methodology," Journal of Power Sources, vol. 399, pp. 314–328, Sep. 2018, doi: 10.1016/j.jpowsour.2018.06.098.

[21] J. Liu, Q. Li, W. Chen, Y. Yan, Y. Qiu, and T. Cao, "Remaining useful life prediction of PEMFC based on long short-term memory recurrent neural networks," International Journal of Hydrogen Energy, vol. 44, no. 11, pp. 5470–5480, Feb. 2019, doi: 10.1016/j.ijhydene.2018.10.042.

[22] B. Long, K. Wu, P. Li, and M. Li, "A Novel Remaining Useful Life Prediction Method for Hydrogen Fuel Cells Based on the Gated Recurrent Unit Neural Network," Applied Sciences, vol. 12, no. 1, p. 432, Jan. 2022.

[23] C. Wang, M. Dou, Z. Li, R. Outbib, D. Zhao, and B. Liang, "A fusion prognostics strategy for fuel cells operating under dynamic conditions," *eTransportation*, vol. 12, p. 100166, May 2022.

[24] C. Wang *et al.*, "Data-driven prognostics based on time-frequency analysis and symbolic recurrent neural network for fuel cells under dynamic load," *Reliability Engineering & System Safety*, vol. 233, p. 109123, May 2023, doi: 10.1016/j.ress.2023.109123.

[25] H. Liu, J. Chen, D. Hissel, J. Lu, M. Hou, and Z. Shao, "Prognostics methods and degradation indexes of proton exchange membrane fuel cells: A review," *Renewable and Sustainable Energy Reviews*, vol. 123, p. 109721, May 2020, doi: 10.1016/j.rser.2020.109721.

[26] R. Ma, R. Xie, L. Xu, Y. Huangfu, and Y. Li, "A Hybrid Prognostic Method for PEMFC With Aging Parameter Prediction," *IEEE Trans. Transp. Electrific.*, vol. 7, no. 4, pp. 2318–2331, Dec. 2021.

[27] D. Zhou, F. Gao, E. Breaz, A. Ravey, and A. Miraoui, "Degradation prediction of PEM fuel cell using a moving window based hybrid prognostic approach," *Energy*, vol. 138, pp. 1175–1186, Nov. 2017.

[28] Y. Wang et al., "Degradation prediction of proton exchange membrane fuel cell stack using semi-empirical and data-driven methods," Energy and AI, vol. 11, p. 100205, Jan. 2023, doi: 10.1016/j.egyai.2022.100205.

[29] Z. Tian, J. Wang, A. Al-Durra, S. M. Muyeen, D. Zhou, and S. Hua, "A novel aging prediction method of fuel cell based on empirical mode decomposition and complexity threshold quantitative criterion," Journal of Power Sources, vol. 574, p. 233120, Aug. 2023, doi: 10.1016/j.jpowsour.2023.233120.

[30] H. Liu, J. Chen, D. Hissel, and H. Su, "Remaining useful life estimation for proton exchange membrane fuel cells using a hybrid method," *Applied Energy*, vol. 237, pp. 910–919, Mar. 2019.

[31] M. S. Jha, M. Bressel, B. Ould-Bouamama, and G. Dauphin-Tanguy, "Particle filter based hybrid prognostics of proton exchange membrane fuel cell in bond graph framework," *Computers & Chemical Engineering*, vol. 95, pp. 216–230, Dec. 2016.

[32] M. Bressel, M. Hilairet, D. Hissel, and B. Ould Bouamama, "Extended Kalman Filter for prognostic of Proton Exchange Membrane Fuel Cell," *Applied Energy*, vol. 164, pp. 220–227, Feb. 2016.

[33] R. Pan, D. Yang, Y. Wang, and Z. Chen, "Performance degradation prediction of proton exchange membrane fuel cell using a hybrid prognostic approach," *International Journal of Hydrogen Energy*, vol. 45, no. 55, pp. 30994–31008, Nov. 2020.

[34] M. Jouin, R. Gouriveau, D. Hissel, M.-C. Pera, and N. Zerhouni, "Joint Particle Filters Prognostics for Proton Exchange Membrane Fuel Cell Power Prediction at Constant Current Solicitation," *IEEE Trans. Rel.*, vol. 65, no. 1, pp. 336–349, Mar. 2016, doi: 10.1109/TR.2015.2454499.

[35] S. Han, Z. Meng, X. Zhang, and Y. Yan, "Hybrid Deep Recurrent Neural Networks for Noise Reduction of MEMS-IMU with Static and Dynamic Conditions," *Micromachines*, vol. 12, no. 2, p. 214, Feb. 2021.

[36] W. Shu, F. Zeng, Z. Ling, J. Liu, T. Lu, and G. Chen, "Resource Demand Prediction of Cloud Workloads Using an Attention-based GRU Model," in *2021 17th Int. Conf. Mobility, Sensing Netw. (MSN)*, Exeter, United Kingdom: IEEE, Dec. 2021, pp. 428–437.

[37] "FCLAB Research. IEEE PHM 2014 data challenge. 2014. http://eng.fclab.fr/ieee- phm-2014-data-challenge/.".

[38] M. Jouin, R. Gouriveau, D. Hissel, M.-C. Péra, and N. Zerhouni, "Prognostics of Proton Exchange Membrane Fuel Cell stack in a particle filtering framework including characterization disturbances and voltage recovery," in *2014 Int. Conf. Progno. Health Manag.*, Jun. 2014, pp. 1–6.

[39] K. Benaggoune, M. Yue, S. Jemei, and N. Zerhouni, "A data-driven method for multi-step-ahead prediction and long-term prognostics of proton exchange membrane fuel cell," *Applied Energy*, vol. 313, p. 118835, May 2022, doi: 10.1016/j.apenergy.2022.118835.

[40] Y. Zhang, R. Ma, R. Xie, Z. Feng, B. Liang, and Y. Li, "A Degradation Prediction Method for PEM Fuel Cell Based on Deep Temporal Feature Extraction and Transfer Learning," IEEE Trans. Transp. Electrific., pp. 1–1, 2023, doi: 10.1109/TTE.2023.3262588.

[41] K. He, C. Zhang, Q. He, Q. Wu, L. Jackson, and L. Mao, "Effectiveness of PEMFC historical state and operating mode in PEMFC prognosis," International Journal of Hydrogen Energy, vol. 45, no. 56, pp. 32355–32366, Nov. 2020, doi: 10.1016/j.ijhydene.2020.08.149.